

Modelling impingement of hollow metal droplets onto a flat surface

Arvind Kumar, Sai Gu*

School of Engineering Sciences, University of Southampton, Highfield, Southampton SO17 1BJ, UK

ARTICLE INFO

Article history:

Received 28 December 2011
Received in revised form 29 April 2012
Accepted 7 June 2012
Available online 2 July 2012

Keywords:

Thermal spray coating
Hollow droplet
Solidification
Volume of fluid
One-domain formulation
Transient
CFD

ABSTRACT

Despite many theoretical and experimental works dealing with the impact of dense melt droplets on the substrate during the process of thermal spray coating, the dynamics of the impingement of hollow melt droplet and the subsequent splat formation are not well addressed. In this paper a model study for the dynamic impingement of hollow droplet is presented. The hollow droplet is modelled such that it consists of a liquid shell enclosing a gas cavity. The impingement model considers the transient flow dynamics during impact, spreading and solidification of the droplet using the volume of fluid surface tracking method (VOF) coupled with a solidification model within a one-domain continuum formulation. The results for spreading, solidification and formation of splats clearly show that the impingement process of hollow droplet is distinctly different from the dense droplet. Study with different droplet void fractions and void distribution indicates that void fraction and void distribution have a significant influence on the flow dynamics during impact and on the final splat shape. The results are likely to provide insights for the less-explored behaviour of hollow melt droplets in thermal spray coating processes.

© 2012 Elsevier Inc. All rights reserved.

1. Introduction

The principle of droplet impingement on the solid surface has been applied to many engineering applications. For example, the purpose of thermal spray coating is to melt powder particles and project them onto substrates to produce protective coating. The quality of the coating is a direct outcome of the impingement process in which individual splats are formed. The impingement process depends on several factors such as, particle impact velocity, particle size, particle material properties, wetting of the substrate by molten particles, substrate temperature and roughness. While experimental investigations can link these factors to a final coating morphology, computer simulations are now providing further scientific insight to the impingement process, the physics of the coating build up and in tuning the process parameters. Therefore significant effort is being devoted to the modelling and simulation of the particle impingement process (Pasandideh-Fard et al., 1998, 2002; Aziz and Chandra, 2000; Ahmed and Rangel, 2002; Shakeri and Chandra, 2002; Kamnis and Gu, 2005; Yang et al., 2011; Kamnis et al., 2008; Shi et al., 2004; Li and Christofides, 2005; Berberovic et al., 2011; Bhardwaj and Attinger, 2008).

The modelling of fully molten droplet impingement has improved the understanding of particle deformation and adhesion in thermal spraying. These works are well reviewed by Kamnis and Gu (2005), and Chandra and Fauchais (2009). At present the latest models are capable of describing several physical phenom-

ena which arise during the process of molten droplet impingement. Computational fluid dynamics (CFD) based volume of fluid method (VOF) is utilized in many cases to track the deforming surface of the molten droplet (Pasandideh-Fard et al., 2002; Ahmed and Rangel, 2002; Kamnis and Gu, 2005; Kamnis et al., 2008). The fluid surface tension force at the boundary between the droplet and the surrounding gas is included as a body force in the momentum conservation equation (Pasandideh-Fard et al., 2002; Kamnis and Gu, 2005). Solidification of the droplet has been considered using different methods. The decrease in velocity due to solidification may be mathematically described by introducing a Darcy sink term within the momentum conservation equation (Kamnis and Gu, 2005). Alternatively, a fixed velocity method is adopted by Pasandideh-Fard et al. (1998), whereby the velocity vector within the momentum conservation equation is directly multiplied by the liquid phase fraction within the associated computational cell. Hence, if the cell is fully solid then the contents of the cell are stationary. The works in Pasandideh-Fard et al. (1998), Ahmed and Rangel (2002), Kamnis and Gu (2005) couple the heat energy transfer between the droplet and the substrate which plays a vital role in simulating the splat morphology by controlling the rate of cooling and solidification. The more advanced computational models include a thermal contact resistance (Pasandideh-Fard et al., 1998; Kamnis and Gu, 2005), which is physically created by the air enclosed within the roughness of the substrate and acts as a resistance to the coupled heat transfer process. Validation of these models has highlighted their ability to successfully predict the rate of spreading and solidification of a single molten droplet impingement (Pasandideh-Fard et al., 1998; Kamnis and Gu,

* Corresponding author.

E-mail address: s.gu@soton.ac.uk (S. Gu).

List of Symbols

c	specific heat capacity, $\text{J kg}^{-1}/\text{K}$	\vec{u}	continuum velocity vector, m/s
C	constant related to Darcy source term, $\text{kg m}^{-3}/\text{s}$	<i>Greek symbols</i>	
D_0	initial droplet diameter, m	μ	dynamic viscosity, $\text{kg m}^{-1}/\text{s}$
d	initial void diameter, m	ρ	density, kg/m^3
f_l	weight fraction of liquid	<i>Subscript</i>	
f_s	weight fraction of solid	d	droplet
F	volume of fluid function	w	wall (substrate)
\vec{g}	acceleration due to gravity vector, m/s^2	air	air
g_l	volume fraction of liquid	eff	effective
g_s	volume fraction of solid	l	liquid
k	thermal conductivity, $\text{W m}^{-1}/\text{K}$	0	initial
L	latent heat of fusion, J/kg	s	solid
t	time, s		
T	temperature, K		
U_0	droplet's initial vertical downward velocity, m/s		

2005) with the correct number of fingers surrounding a three dimensional splat (Kamnis et al., 2008). The above-mentioned theoretical studies for impingement of droplets assume that the particle is in a spherical shape without voids inside.

New possibilities for thermal spraying of functional coatings formed by deposition of hollow melt droplets are discussed in the work by Solonenko et al. (2008a, 2008b, 2011). The high-velocity impact of a hollow droplet onto the substrate and the splat formation can differ fundamentally from the conventional dense droplet. The presence of voids in the feedstock powders can also have a great impact on particle in-flight behaviours such as particle acceleration, melting and oxidation because a hollow particle is also lighter than a continuous particle. This can affect the particle trajectory. Very recently, computational results for HVOF sprayed porous WC-Co powder indicate that these particles are accelerated to higher velocity with higher surface temperatures than fully solid powders (Kamnis et al., 2011). The hollow and particles can be obtained by plasma processing of powder materials (Solonenko et al., 2008a, 2008b; Solonenko et al., 2011), where they formed from spray dried agglomerates. These hollow powder particles having voids, during their in-flight motion in the course of the coating process, form hollow liquid droplets prior to their impact with the substrate. Shinoda and Murakami (2010) studied the splat morphology of yttria-stabilized zirconia (YSZ) droplets using dense and hollow spherical powders. Gao et al. (2008) employed three nanostructured WC-12Co powders with different porous structure to deposit WC-Co coatings on stainless steel substrate by cold spraying. They found that WC-Co coating is easily built-up using porous powders. In the work of Chien and Coyle (2007) deposition of porous nanocrystalline SnO_2 coating with interpenetrating pores for gas sensor applications was studied.

The limited studies in this field (Solonenko et al., 2008a,b; Gao et al., 2008) suggest that the resulting coating is characterized by a more stratified structure, which opens up new prospects for the application of hollow powders for making thermal coatings with substantially improved characteristics (e.g., adhesion, structure uniformity, etc.) In plasma spraying, the main disadvantage of powders made up by dense continuous particles is that, even with known particle surface temperature, one cannot be certain that the particles were molten completely in the plasma jet because the temperature gradients inside the particles are high. On the contrary, in the spraying of hollow particles, it can be guaranteed that the 5–10 μm thick shell material in such particles undergoes complete melting, with the temperature being quite uniform across the particle (Solonenko et al., 2008a,b). In this connection, the investigation of the impingement of a hollow melt droplet onto a solid substrate is of scientific and applied importance.

Despite many theoretical and experimental works dealing with the dense melt droplets, the dynamics of the impingement of hollow melt droplet and the subsequent splat formation are not well addressed and hence the current understanding of the behaviour of hollow particles in thermal spray is very limited. A clear understanding of the impingement behaviour of hollow droplet on the surface of substrates is needed in order to better control the splat formation and the coating structure using the hollow particles. This study builds upon previous work of Kamnis and Gu (2005) and Kamnis et al. (2008) on the well validated impingement process of dense droplets. The purpose of this work is to develop a numerical model for the impingement of a hollow droplet and to reveal the underlying physics of the process, which will shed light on the essential parameters and the phenomena of the splat formation during the use of hollow particles in thermal spray coating. In the impingement model transient flow dynamics during impact, simultaneous spreading and solidification are considered using the volume of fluid surface tracking method (VOF) coupled with a solidification model within a one-domain continuum formulation. The hollow droplet impact, spreading, solidification and formation of splats on a flat surface are simulated. The features of hollow droplets impact including its subsequent spreading and formation of the splat on the substrate are discussed in detail. The results indicate that the impingement process of hollow droplet is distinctly different from the analogous dense droplet. The influence of the droplet void fraction on the impingement behaviour is also discussed.

2. Problem description and numerical model

We consider the problem corresponding to the benchmark experimental conditions for the impingement of a dense droplet as reported in Shakeri and Chandra (2002). The current study is focused to investigate the impingement behaviour of a hollow droplet where immediately prior to droplet-substrate collision, the droplet consists of a liquid shell enclosing a gas cavity. The computational parameters chosen allow a comparison of the results of the hollow droplet impact with the results of the continuous droplet impact, and thus clearly establishing the dynamics of the hollow droplet impact. For this a molten tin hollow spherical droplet with an outer diameter (D_0) 2.2 mm and void (of air) diameter (d) 1.1 mm at an initial uniform temperature of 519 K is considered to impinge with a velocity of 4 m/s onto a flat, stainless steel substrate kept at an initial temperature of 298 K. This hollow droplet ($d/D_0 = 0.5$) results in 50% void in terms of the circular size and

12.5% void in terms of the spherical mass of the droplet. The value of the Bi number for the molten droplet without voids travelling through air is well below unity (0.011). This justification has then been applied to include an initial uniform temperature distribution inside the droplet with voids. We have considered a 2D axisymmetric formulation and Fig. 1 shows the schematic of the computational domain. The domain consists of 240,000 structured computational cells with a refined mesh at the substrate surface. The numerical methodology is based on the previously validated model for a dense droplet (Kamnis and Gu, 2005). The accuracy of the dense droplet impingement model reported in the work of Kamnis and Gu (2005) was validated with the experimental measurement of tin droplets (Shakeri and Chandra, 2002). Upon impingement, the transfer of heat is dominated by convection and conduction, and hence radiation from the droplet surface to the surroundings is not considered (Kamnis and Gu, 2005). Table 1 shows the material properties, taken from Kamnis and Gu (2005), for the current problem.

2.1. Mathematical formulation

2.1.1. Free surface modelling

The VOF model is used to track the interface between the droplet and the air considering these two as immiscible fluids by solving a single set of momentum equations. This method tracks the volume fraction of each of the fluids throughout the computational domain. Accordingly, the governing equations are being solved in both air and molten droplet domains. The volume of fraction of fluid in a control volume (F) has a range from zero to unity; the cells having F values between zero and one ($0 < F < 1$) represent the air–molten droplet interface, $F = 0$ indicates that the cell contains only air, and $F = 1$ corresponds to a cell full of droplet material. The volume of fraction function F is advected using the continuum mixture velocity field \vec{u} with the following transport equation:

$$\frac{\partial F}{\partial t} + \nabla \cdot \vec{u}F = 0 \quad (1)$$

The compressive interface capturing scheme (CICSAM) by Ubbink and Issa (1999) is applied as the discretization scheme because of its suitability for flows with high viscosity ratios between the immiscible phases. The full mathematical description of the CICSAM scheme can be found in Ubbink and Issa (1999).

2.1.2. Momentum and heat transport modelling

In the current model, a continuum formulation with a one-domain approach based on the classical mixture theory (Kamnis and Gu, 2005; Pathak et al., 2009; Yadav et al., 2009) is adopted.

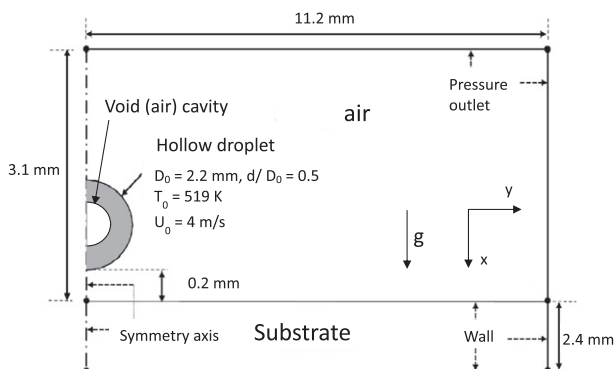


Fig. 1. Schematic diagram of the axisymmetric computational domain.

A cell with molten droplet may consist both the liquid and the solid phase (the mushy state), and we define the following mixture quantities for a cell in the mushy state.

$$g_l + g_s = 1, \quad f_l + f_s = 1, \quad f_l = \frac{g_l \rho_l}{\rho_d}, \quad \rho_d = g_l \rho_l + (1 - g_l) \rho_s \quad (2)$$

where the f_l and g_l are the mass fraction and the volume fraction of liquid in the droplet, respectively. As we consider different density of the solid and the liquid phase, f_l and g_l will be different and are related by the relation given in Eq. (2). Shrinkage will take place because of different solid and liquid phase density and the flow due to the contraction will be compensated by air. The pressure outlet boundary condition considered at the outer part of the computational domain will facilitate this. Next, the volume-fraction-averaged continuum density in each control volume can be calculated according to the fraction of the droplet fluid (F).

$$\rho = F \rho_d + (1 - F) \rho_{air} \quad (3)$$

where the subscripts 'd' and 'air' are for the droplet and the air phase, respectively. The density of air is assumed to be constant in the current model. Other volume-fraction-averaged properties are also defined in a similar manner. The volume-fraction-averaged material properties are then used in the momentum and energy transport equations which are given in the following.

$c_{eff} = F c_d + (1 - F) c_{air}$ same specific heat capacity for solid and liquid part of the droplet

$$k_{eff} = F k_d + (1 - F) k_{air} \quad \text{with } k_d = g_l k_l + (1 - g_l) k_s$$

$$\mu = F \mu_d + (1 - F) \mu_{air} \quad (4)$$

The momentum and energy conservation equations are coupled with the VOF model. Assuming the flow to be Newtonian, incompressible and laminar, the governing equations for mass, momentum and energy conservation can be written as follows.

$$\text{Continuity: } \frac{\partial}{\partial t} (\rho) + \nabla \cdot (\rho \vec{u}) = 0 \quad (5)$$

$$\begin{aligned} \text{Momentum conservation: } & \frac{\partial}{\partial t} (\rho \vec{u}) + \nabla \cdot (\rho \vec{u} \vec{u}) \\ & = -\nabla p + \nabla \cdot [\mu (\nabla \vec{u} + \nabla \vec{u}^T)] \\ & + \rho \vec{g} + F_{vol} - S \vec{u} \end{aligned} \quad (6)$$

For cells which are undergoing phase change, the interaction force term is evaluated using Darcy's model of viscous flow through a porous medium (Kamnis and Gu, 2005; Pathak et al., 2009; Yadav et al., 2009). The source term Su is used to modify the momentum equation in a mushy zone (a region in which the liquid fraction lies between 0 and 1). This source term acts such that as the mush porosity decreases the velocity also decreases to zero when the mush becomes completely solid (Kamnis and Gu, 2005; Pathak et al., 2009; Yadav et al., 2009). This term is active only for cells filled with molten droplet and vanishes at the free surface and in the air phase. This term is given as

$$S \vec{u} = \begin{cases} \left[C \frac{(1-g_l)^2}{g_l^3} \right] \vec{u} & F = 1 \\ 0 & F < 1 \end{cases} \quad (7)$$

where C is a constant accounting for the solidification phase morphology. In the current model C is assumed a constant value of 150,000 (Kamnis and Gu, 2005). In the current fixed-grid one-domain approach (Kamnis et al., 2008; Pathak et al., 2009) the liquid–solid interface is not needed to be tracked separately. In this method, the liquid–solid interface is obtained as the solution of the governing equations, and is estimated based on the local solid

Table 1
Material properties.

Impinging droplet material	Tin (Sn)
Substrate material	Stainless steel (SS)
Gas phase (the void and the droplet surrounding medium)	Air (air)
Droplet initial temperature	519 K
Substrate initial temperature	298 K
Solidus temperature (Sn)	504 K
Liquidus temperature (Sn)	506 K
Thermal conductivity (liquid Sn)	33.6 W m ⁻¹ /K
Thermal conductivity (solid Sn)	62.2 W m ⁻¹ /K
Thermal conductivity (SS)	14.9 W m ⁻¹ /K
Thermal conductivity (air)	0.0242 W m ⁻¹ /K
Density (liquid Sn)	6980 kg/m ³
Density (solid Sn)	7200 kg/m ³
Density (SS)	7900 kg/m ³
Density (air)	1.225 kg/m ³
Droplet surface tension	0.566 N/m
Viscosity (liquid Sn)	0.0022 kg m ⁻¹ /s
Viscosity (air)	1.7894 × 10 ⁻⁵ kg m ⁻¹ /s
Specific heat capacity (solid and liquid Sn)	244 J kg ⁻¹ /K
Specific heat capacity (SS)	477 J kg ⁻¹ /K
Specific heat capacity (air)	1006.43 J kg ⁻¹ /K ¹
Latent heat of fusion	58500 J/kg

fraction in the computational cell. Momentum conservation equation also includes a body force, F_{vol} , accounting for surface tension effects at the free surface, which is formulated by the continuum surface force model (CSF) of Brackbill et al. (1992) using the fluid densities at the interface and the droplet surface tension. The formulation and the numerical implementation are described in detail in (Kamnis and Gu, 2005). The values considered for the liquid–solid contact angle during droplet advancing and receding are same as those given in our previous work (Kamnis and Gu, 2005).

$$\text{Energy conservation : } \frac{\partial}{\partial t}(\rho c_{eff}T) + \nabla \cdot (\rho \vec{u} c_{eff}T) = \nabla \cdot (k_{eff} \nabla T) + S_h \quad (8)$$

$$S_h = \begin{cases} -L \left[\frac{\partial}{\partial t}(\rho f_i) + \nabla \cdot (\rho \vec{u} f_i) \right] & F = 1 \\ 0 & F < 1 \end{cases} \quad (9)$$

where L is the latent heat of fusion. The source term S_h is active only for the cells filled with molten droplet, i.e. for $F = 1$. The local liquid fraction f_i in a computational cell is calculated from the local temperature as

$$f_i = \begin{cases} 0 & \text{if } T \leq T_{solidus} \\ 1 & \text{if } T \geq T_{liquidus} \\ \frac{T - T_{solidus}}{T_{liquidus} - T_{solidus}} & \text{if } T_{solidus} < T < T_{liquidus} \end{cases} \quad (10)$$

It may be noted that due to high temperature difference between the droplet and substrate and the relative low droplet velocity (Eckert number: $U_0^2/c\Delta T \approx 3 \times 10^{-4}$), viscous dissipation is negligible and hence it is not included in the current model (Kamnis and Gu, 2005). In the substrate only heat transfer equation is solved where the mode of heat transfer is conduction. In reality air is entrapped within the roughness of the material surface which acts as thermal resistance. The model takes into account the air entrapment by applying a thermal resistance to the flow of heat energy to the substrate. A value of $1.8 \times 10^{-6} \text{ m}^2 \text{ K W}^{-1}$ for the thermal contact resistance is applied which corresponds to a stainless steel substrate roughness of $0.06 \mu\text{m}$ (Shakeri and Chandra, 2002). The boundary condition at the side and the bottom of substrate is a fixed temperature of 298 K. The governing equation in the substrate is given as

$$\frac{\partial}{\partial t}(\rho_w c_w T) = \nabla \cdot (k_w \nabla T) \quad (11)$$

The initial conditions appropriate to the physical system shown in Fig. 1 are: at $t=0$, droplet temperature (void and shell) $T_d = 519 \text{ K}$, $F = 1$ in the droplet shell, $F = 0$ in the droplet void; droplet velocity = 4 m/s; $u = v = F = 0$, $T = 298 \text{ K}$ everywhere else in the domain. It may be noted that the void in the hollow droplet is of the same gas which surrounds the droplet (i.e., air). Boundary conditions for the problem considered are shown in Fig. 1.

3. Results and discussion

3.1. Impingement behaviour

The dynamic impingement process of the hollow droplet ($d/D_0 = 0.5$) is shown in Fig. 2. For the purpose of comparison, result for the spreading of the same-size dense droplet (diameter $D_0 = 2.2 \text{ mm}$) is also displayed side-by-side. This case for the hollow droplet implies 50% void (in terms of the circular size) in the droplet. However, in terms of the mass of the spherical droplet it implies 12.5% void. After the impact the dense droplet spreads radially along the substrate surface (Fig. 2a). It was noticed that the droplet reaches its maximum spread at 1.8 ms which will be quantitatively illustrated subsequently in Fig. 5. After this surface tension pulls the edges of the droplet inwards and the spreading stabilizes from 5 ms when the droplet mainly solidifies. This typical spreading and solidification behaviour for a dense droplet is reported in detail in (Kamnis and Gu, 2005) and hence the descriptions are not repeated here.

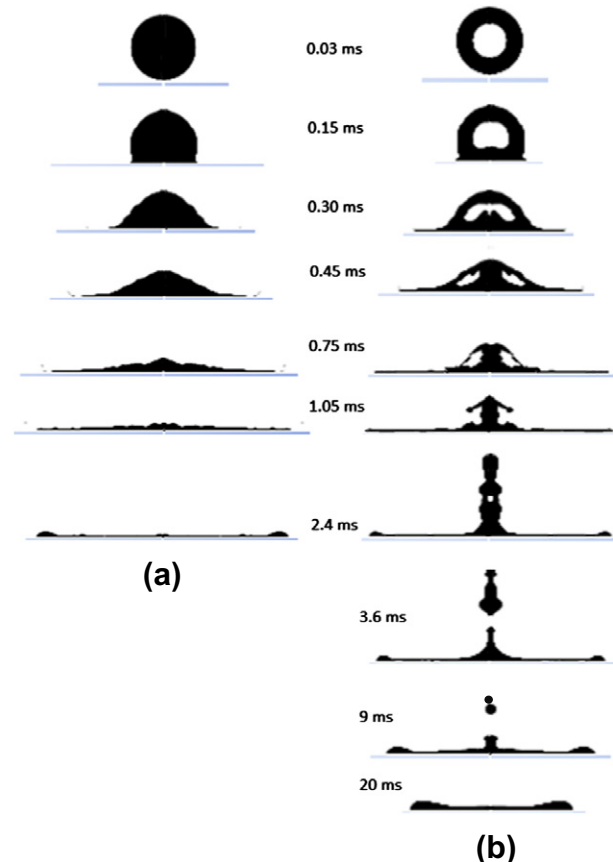


Fig. 2. Snapshots of droplet spreading on the substrate (a) dense droplet and (b) hollow droplet ($d/D_0 = 0.5$).

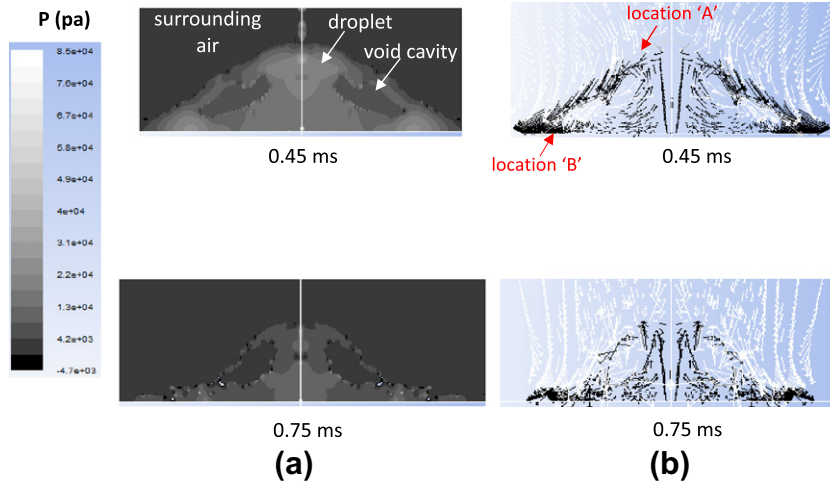


Fig. 3. (a) Gauge pressure and (b) velocity distribution in the hollow droplet. The white colour velocity vectors are in the air (surrounding and void cavity) and the black colour in the droplet.

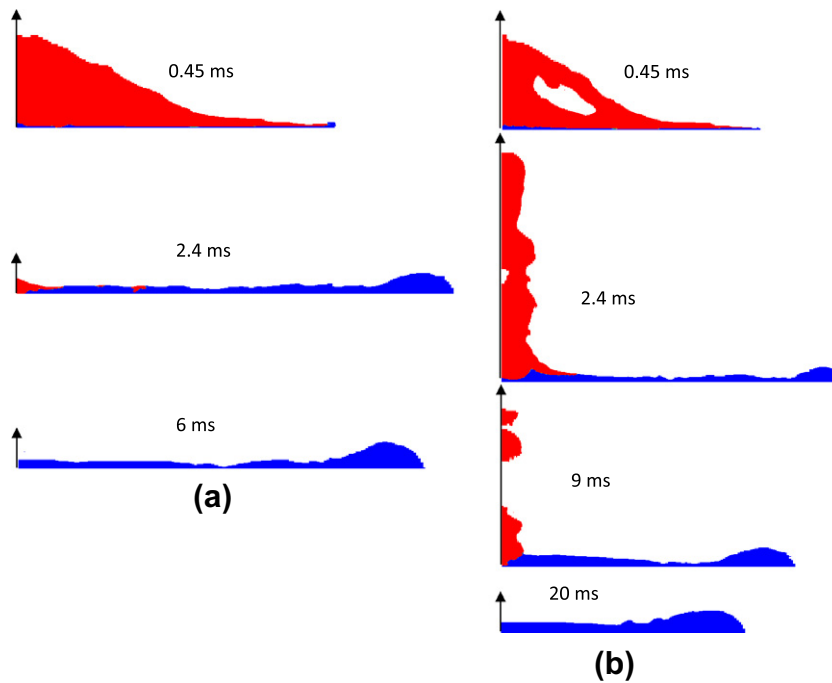


Fig. 4. Snapshots of droplet solidification (a) dense droplet and (b) hollow droplet ($d/D_0 = 0.5$). Only half of the axisymmetric domain is shown. The blue colour shows zone with liquid fraction lower than one (mushy or fully solid) and the red colour shows fully liquid zone. The droplet–air interface is the boundary of the red colour. (For interpretation of the references to colour in this figure legend, the reader is referred to the web version of this article.)

The hollow droplet (Fig. 2b) also show similar spreading except the fact that the void within the hollow droplet undergo deformation (0.15 ms), stretching (0.30 ms), disintegration into two void cavities (0.45 ms) and finally rupture of the two void cavities (0.75 ms). At the *first stage* of the impingement process the lower hemispherical shell comes into contact with the substrate surface and progressively deforms. At the same time, the upper hemispherical shell proceeds with the motion with initial velocity. At the *second stage* rupture occurs at the periphery of the upper hemisphere. At the *third stage* the upward movement of the central splash of the droplet (1.05 ms) takes place. Such counter jetting phenomenon and the central splash found in our simulation is similar to that observed in the experiment reported by Gulyaev et al. (2009) for the hollow droplet impingement. Experiments

reported for visualization of the collision of a hollow liquid drop with a flat surface showed that the impact leads to the formation of a central counter jet of the liquid (Gulyaev et al., 2009). The upward moving central counter liquid jet finally detaches from the lower part (3.6 ms) and keeps moving in upward direction before it loses its upward momentum. After this the detached part starts to fall upon the solidifying splat (9 ms) and finally solidifies (20 ms). It was estimated that the droplet spreading on the substrate reaches its maximum spread at 1.35 ms (this will be quantitatively illustrated in Fig. 5 shown subsequently). After this surface tension pulls the edges of the droplet inwards and the spreading stabilizes from 15 ms when the droplet mainly solidifies.

In order to illustrate the cause of the formation of central counter jetting we show the pressure (gauge pressure) and the velocity

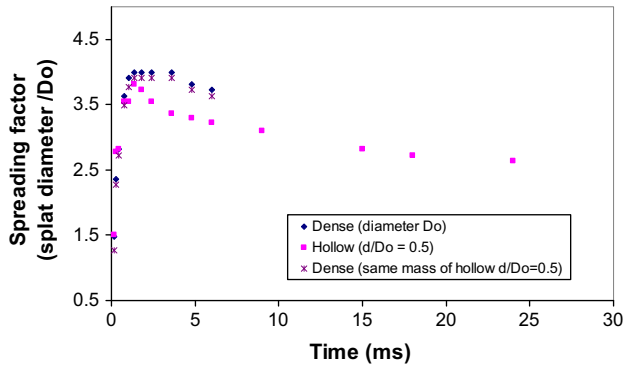


Fig. 5. Comparison of droplet spreading factor for hollow and dense droplet.

distributions in the droplet in Fig. 3. We noticed that at 0.45 ms when the void disintegrates into two pieces the flow from the top of the void (location 'A') follows the spreading path (Fig. 3b). However, there is also a backward vortex from the periphery of the bottom part (location 'B') towards the centre of droplet. This backward flow is caused by a pressure build up near location 'B' at the periphery (Fig. 3a). Subsequently, when rupture of the void occurs at 0.75 ms the pressure build up location shifts towards the centre of the droplet and the backward vortex, generated earlier, creates an upward flow at the centre of the droplet. From location 'B' a part of the liquid flows toward the centre, that generates a radial converging liquid stream. This creates the central counter jet. Liquid is continuously supplied to the counter jet from the shell. Meanwhile, the radial converging flow in the central counter jet that is directed along the outer normal to the substrate creates an upward movement of the counter jet.

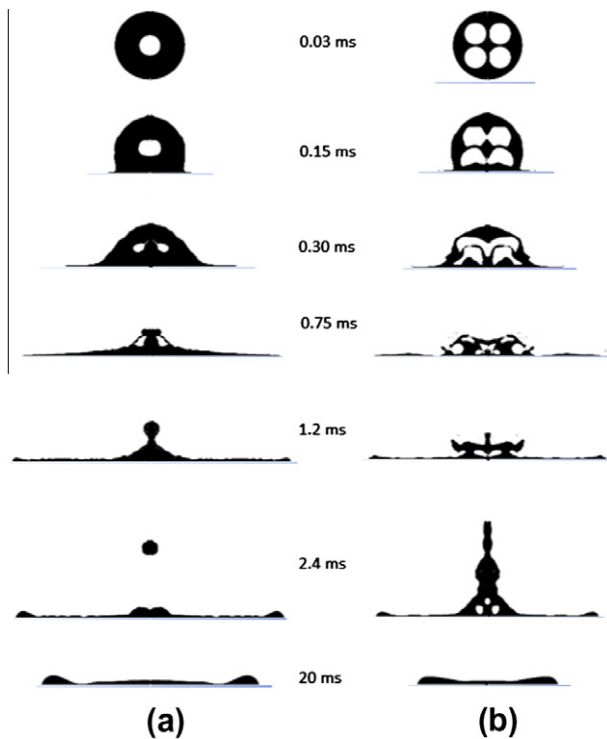


Fig. 6. Snapshots of droplet spreading for different void fraction (a) hollow droplet ($d/D_0 = 0.3$) and (b) hollow droplet with four small distributed voids having the same mass as that of $d/D_0 = 0.5$ hollow droplet.

3.2. Solidification behaviour

The snapshots of droplet solidification for the dense and the hollow droplet ($d/D_0 = 0.5$) are shown in Fig. 4. It may be noted that in this figure only the axisymmetric half is shown. For the dense droplet a thin solidification layer is developed at the substrate surface at 0.45 ms. This solidification layer increases in size (height and diameter) as the droplet spreads. At 2.4 ms only a small fraction of the droplet remains in fully liquid state. In the remaining part of the droplet (shown in blue colour) the part adjacent to the substrate is fully solid and the part above this is in mushy state. In the mushy part the flow due to surface tension at the edges pulls the droplet edge inwards which decreases the diameter of the splat (Kamnis and Gu, 2005). The droplet solidifies fully at 6 ms. For the case of hollow droplet a similar behaviour of the solidifying zone is observed except the fact that the part of the droplet in fully liquid state is relatively much larger because of the upward motion of the central splash and its detachment from the bottom splat. This causes the detached part to remain not in contact with the bottom splat for a long time. This reduces the heat extraction from the detached part and accordingly, the final solidification time for the hollow droplet is much larger (20 ms) than the dense droplet (6 ms).

From the distinctly different impingement process of the dense and the hollow droplet, as described in Figs. 2 and 4, we can qualitatively note the following main features of a hollow droplet. The hollow droplet results in a large central splash during the impingement process, a smaller final splat diameter, a larger-sized rim and a thicker and more uniform splat than a dense droplet. The term 'uniform splat' is mentioned in the sense when the difference in the rim size and the central part of the splat is smaller. As seen in Fig. 4, as compared to the dense droplet the hollow droplet spreads slowly along the substrate. This is because of the formation of a large central counter liquid jet with the hollow droplet, which reduces the amount of the droplet available for spreading along the substrate. The counter jet slowly falls and moves smoothly upon a solidified splat (9 ms). These factors lead to a smaller and uniform final splat in the case of the hollow droplet.

Fig. 5 shows the quantitative comparison of the transient spread factor for the case of the hollow and the dense droplet. In this figure the results of an analogous dense droplet having same mass as that of the hollow droplet is also included. Based on a spherical shape of the droplet, this dense droplet will have the diameter of $0.956D_0$ for having the same mass as that of the hollow droplet. Accordingly, Fig. 5 includes results of a hollow droplet ($d/D_0 = 0.5$), same size dense droplet (diameter = D_0) and same mass dense droplet (diameter = $0.956D_0$). The spread factor is defined as the ratio of the instantaneous splat diameter to D_0 ($=2.2$ mm).

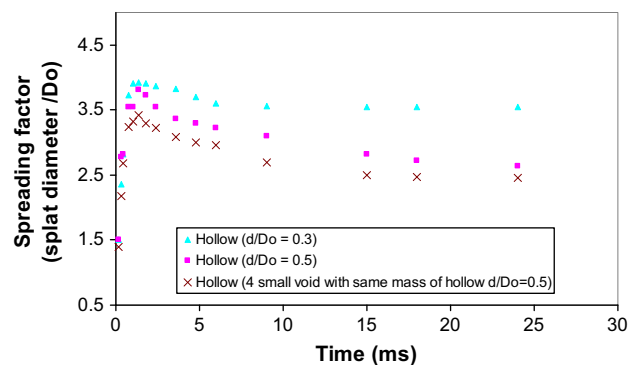


Fig. 7. Comparison of spreading factor for hollow droplet with different void fraction.

From this figure we can quantitatively notice that the hollow droplet results in smaller splat diameter (about 30% smaller) compared to the dense droplet.

3.3. Influence of void fraction and void distribution

In the following results for the influence of the void fraction and the void distribution in the hollow droplet on the impingement process are presented. Simulations for two other hollow droplets are performed: (i) $d/D_0 = 0.3$ resulting in 30% void in terms of the circular size and 2.7% void in terms of the mass and (ii) hollow droplet with four small distributed voids having the same droplet mass (and hence the same void fraction in terms of mass) as that of $d/D_0 = 0.5$ hollow droplet case. It may be noted that in these simulations we maintained D_0 as 2.2 mm. Fig. 6 displays the dynamic impingement process for these two cases. Comparing Fig. 6a with Fig. 2b we can notice that the hollow droplet with lower void fraction (i.e., $d/D_0 = 0.3$ case) results in a similar evolution of the impingement process as that of $d/D_0 = 0.5$ hollow droplet. However, the notable observation is that even a lower void fraction (i.e., 2.7%) can result in differences in the droplet impingement process and in the final splat shape and size as compared to the dense droplet (see Figs. 2a and 6a). Overall, the uniformity of the splat improves and size reduces as the void fraction increase. From Fig. 6b we can notice that the distributed voids results in even more uniform splat (see Figs. 2b and 6b). The impingement process with the distributed voids follows the typical stages of the impingement as that of the single void as described earlier. The final splat diameter is found to be smaller with the distributed voids (see Figs. 2b and 6b).

Fig. 7 displays the comparison of the transient spread factor for different simulations of hollow droplets. From this figure we can quantitatively notice that increasing the void fraction results in smaller splat diameter. The splat diameter reduces further when the voids are distributed.

4. Conclusion

The paper presented includes a model to describe the impingement behaviour of a hollow droplet onto a substrate and the results of computer simulations. The results for spreading, solidification and formation of splats clearly show that the impingement process of hollow droplet is distinctly different from the dense droplet. The void in the droplet causes a phenomenon of counter jetting during the impact, similar to that found in experiment, which subsequently detaches from the remaining droplet. In the current study, the hollow droplet results in a large central splash, a smaller final splat diameter, a larger-sized rim and a thicker and more uniform splat as compared to the dense droplet. The solidification time for the splat formed with hollow droplet is also relatively large. It is also found that the final splat shape and size is significantly dependent on the void fraction. The current study shows that even a lower void fraction (for example, 2.7% void in terms of mass) caused differences in the droplet impingement process and in the final splat shape and size as compared to the dense droplet. Higher void fraction results in smaller and more uniform splat. The splat size decreases and splat uniformity increases further when voids are distributed. These results are expected to provide insights to the impact and the solidification behaviour during the deposition of hollow melt droplets onto the

substrates. Our future work will focus on deposition parameters typically seen in thermal spray coating processes.

Acknowledgement

The authors gratefully acknowledge the financial support from the EC FP7 Simuspray project (Grant No. 230715).

References

- Ahmed, A.M., Rangel, R.H., 2002. Metal droplet deposition on non-flat surfaces: effects of substrate morphology. *Int. J. Heat Mass Transfer* 45, 1077–1091.
- Aziz, S.D., Chandra, S., 2000. Impact, recoil and splashing of molten metal droplets. *Int. J. Heat Mass Transfer* 43, 2841–2857.
- Berberovic, E., Roisman, I.V., Jakirlic, S., Tropea, C., 2011. Inertia dominated flow and heat transfer in liquid drop spreading on a hot substrate. *Int. J. Heat Fluid Flow* 32, 785–795.
- Bhardwaj, R., Attinger, D., 2008. Non-isothermal wetting during impact of millimeter-size water drop on a flat substrate: numerical investigation and comparison with high-speed visualization experiments. *Int. J. Heat Fluid Flow* 29, 1422–1435.
- Brackbill, J.U., Kothe, D.B., Zemach, C., 1992. A continuum method for modeling surface tension. *J. Comput. Phys.* 100, 335–354.
- Chandra, S., Fauchais, P., 2009. Formation of solid splats during thermal spray deposition. *J. Therm. Spray Tech.* 18, 148–180.
- Chien, K., Coyle, T.W., 2007. Rapid and continuous deposition of porous nanocrystalline SnO₂ coating with interpenetrating pores for gas sensor applications. *J. Therm. Spray Tech.* 16, 886–892.
- Gao, Pei-Hu, Li, Yi-Gong, Li, Chang-Jiu, Yang, Guan-Jun, Li, Cheng-Xin, 2008. Influence of powder porous structure on the deposition behavior of cold-sprayed WC-12Co coatings. *J. Therm. Spray Tech.* 17, 742–749.
- Gulyaev, I.P., Solonenko, O.P., Gulyaev, P.Yu., Smirnov, A.V., 2009. Hydrodynamic features of the impact of a hollow spherical drop on a flat surface. *Tech. Phys. Lett.* 35, 885–888.
- Kamnis, S., Gu, S., 2005. Numerical modelling of droplet impingement. *J. Phys. D: Appl. Phys.* 38, 3664–3673.
- Kamnis, S., Gu, S., Lu, T.J., Chen, C., 2008. Numerical modelling of sequential droplet impingements. *J. Phys. D: Appl. Phys.* 41, 165303, 7p.
- Kamnis, S., Gu, S., Vardavoulias, M., 2011. Numerical study to examine the effect of porosity on in-flight particle dynamics. *J. Therm. Spray Tech.* 20, 630–637.
- Li, M., Christofides, P.D., 2005. Multi-scale modeling and analysis of an industrial HVOF thermal spray process. *Chem. Eng. Sci.* 60, 3649–3669.
- Pasandideh-Fard, M., Bhola, R., Chandra, S., Mostaghimi, J., 1998. Deposition of tin droplets on a steel plate: simulations and experiments. *Int. J. Heat Mass Transfer* 41, 2929–2945.
- Pasandideh-Fard, M., Chandra, S., Mostaghimi, J., 2002. A three-dimensional model of droplet impact and solidification. *Int. J. Heat Mass Transfer* 45, 2229–2242.
- Pathak, N., Kumar, A., Yadav, A., Dutta, P., 2009. Effects of mould filling on evolution of the solid-liquid interface during solidification. *Appl. Therm. Eng.* 29, 3669–3678.
- Shakeri, S., Chandra, S., 2002. Splashing of molten tin droplets on a rough steel surface. *Int. J. Heat Mass Transfer* 45, 4561–4575.
- Shi, D., Li, M., Christofides, P.D., 2004. Diamond jet hybrid HVOF thermal spray: rule-based modeling of coating microstructure. *Ind. Eng. Chem. Res.* 43, 3653–3665.
- Shinoda, K., Murakami, H., 2010. Splat morphology of yttria-stabilized zirconia droplet deposited via hybrid plasma spraying. *J. Therm. Spray Tech.* 19, 602–610.
- Solonenko, O.P., Smirnov, A.V., Gulyaev, I.P., 2008a. Spreading and solidification of hollow molten droplet under its impact onto substrate: computer simulation and experiment. In: Tokuyama, M., Oppenheim, I., Nishiyama, H. (Eds.), *AIP Conference Proceedings*, vol. 982, pp. 561–568.
- Solonenko, O.P., Gulyaev, I.P., Smirnov, A.V., 2008b. Plasma processing and deposition of powdered metal oxides consisting of hollow spherical particles. *Tech. Phys. Lett.* 34, 1050–1052.
- Solonenko, O.P., Gulyaev, I.P., Smirnov, A.V., 2011. Thermal plasma processes for production of hollow spherical powders: theory and experiment. *J. Therm. Sci. Technol.* 6, 219–234.
- Ubbink, O., Issa, R.I., 1999. A method for capturing sharp fluid interfaces on arbitrary meshes. *J. Comput. Phys.* 153, 26–50.
- Yadav, A., Pathak, N., Kumar, A., Dutta, P., Sarkar, S., 2009. Effects of the filling process on the evolution of the mushy zone and macrosegregation in alloy casting. *Modell. Simulat. Mater. Sci. Eng.* 17, 035006.
- Yang, K., Ebisuno, Y., Tanaka, K., Fukumoto, M., Yasui, T., Yamada, M., 2011. Verification of the flattening behavior of thermal-sprayed particles and free-falling droplets through controlling ambient pressure. *Surf. Coat. Tech.* 205, 3816–3823.